Experimental demonstration of 9.6 Gbit/s polar coded infrared light communication system

Experimental Demonstration of 9.6 Gbit/s Polar Coded Infrared Light Communication System

Haotian Zheng, *Student Member, IEEE*, Kaiquan Wu, Bin Chen, Jianou Huang, Yu Lei, Chao Li, Alexios Balatsoukas-Stimming, *Member, IEEE*, Zizheng Cao, *Member, IEEE*, and A. M. J. Koonen, *Fellow, IEEE*

***Abstract*— A new inter-frame polar coded modulation scheme is proposed and experimentally demonstrated in an infrared light communication (ILC) system. The scheme utilizes the Monte Carlo (MC) method to jointly design an inter-frame polar code with 16-ary quadrature-amplitude modulation (16QAM) and orthogonal frequency-division multiplexing (OFDM). The indoor transmission of 9.6 Gbit/s 16QAM OFDM signal is experimentally achieved over a 3.2 km single-mode fiber and 0.8 m free space. The experiment results show that the proposed scheme employing a polar code of length 1024 and cyclic redundancy check aided successive cancellation list (CA-SCL) decoding with a list size of 2 resulted in no errors over 10^7 bits. Moreover, the proposed scheme requires negligible extra decoding complexity with respect to its classical counterpart, MC-constructed polar coded modulation. To the best of our knowledge, this is the first experimental demonstration of a polar coded modulation based infrared light communication system.**

***Index Terms*— Infrared light communication, polar codes, inter-frame correlated, BIPCM.**

I. Introduction

With the explosive growth of data-hungry services and the depletion of spectral resources, the tremendous wireless data traffic is a big challenge. Spatial division by small cells enabling spectrum re-use is an effective solution. Some emerging techniques such as 60 GHz millimeter wave communication and optical wireless communication (OWC) are promising candidates which can provide up to 112 Gbit/s wireless connectivity to end users [1]. Although OWC cannot reach out-of-sight devices, it offers much wider license-free bandwidths with respect to radio techniques and is thus a good supplement to help dealing with the heavy data traffic.

There are two major categories of indoor OWC techniques: visible light communication (VLC) and beam-steered infrared light communication (BS-ILC). BS-ILC systems can use existing commercial infrared products to provide each terminal with point-to-point high capacity service. To increase the reliability and reach of BS-ILC links, forward error-correction (FEC) is one of the vital techniques, especially when the received optical power is low and high-order modulation formats are used. Reed-Solomon (RS) codes and convolutional codes (CC) were first applied to OWC [2], [3]. More powerful techniques like turbo codes and low-density parity-check codes (LDPC) are employed to further enhance the transmission reliability [4]. Proposed by Arıkan in 2008, polar codes have attracted significant interest recent years [5]. Due to their numerous advantages, such as their explicit encoding and decoding structures and their good error-correction performance with low-complexity decoding algorithms, polar codes were adopted in the 5G standard. Some previous works have applied polar codes to VLC [6], [7] and proved its superiority over LDPC codes at short and moderate code lengths using cyclic redundancy check (CRC) aided successive cancellation list (CA-SCL) decoding [8]. Short code lengths are generally favored by latency-constrained short-reach OWC systems for their low decoding latency [8]. However, it cannot release the full potential of polar codes as the consequence of small number of polarizations. In order to break through this bottleneck, using CA-SCL as underlying decoder, a class of inter-frame polar coding with dynamic frozen bits was proposed in [9]. Different from conventional polar coding where the encoding/decoding of each frame is independent of each other, the proposed scheme in [9] establishes a relationship between two adjacent frames. By exploiting this correlation in decoding, a remarkable improvement can be achieved in the overall probability of correct decoding with negligible complexity increment compared to conventional polar coding.

This letter experimentally investigates the application of the inter-frame polar coding in an ILC system. More specifically, the Monte Carlo (MC)-constructed inter-frame polar coded modulation scheme is proposed where MC method is utilized to jointly design the inter-frame polar code with 16-ary quadrature-amplitude modulation (16QAM) and orthogonal frequency-division multiplexing (OFDM). The proposed scheme is specified for the ILC system and the proper values of the number of shared bits m are found for polar codes with rate $R = 0.8$ and two lengths $N = 512$ and 1024. Finally, the experimental setup and results are shown, verifying the effectiveness of the proposed scheme in ILC system successfully.

II. Principles

A. Classical Polar Coding

The construction of polar codes exploits the different reliabilities produced through polarizing transformations. A polar

Manuscript received September 1, 2020; revised November 12, 2020; accepted November 16, 2020. Date of publication November 18, 2020; date of current version December 4, 2020. This work was supported in part by the NWO program on Integrated Nanophotonics, in part by the Open Fund of the State Key Laboratory of Optoelectronic Materials and Technologies, SYSU, in part by the Sichuan Science and Technology Program under Grant 2020YFH0108, in part by the Strategic Priority Research Program of Chinese Academy of Sciences under Grant XDB43000000, and in part by the National Key Research and Development Program of China under Grant 2018YFB2201101. *(Corresponding authors: Chao Li; Zizheng Cao.)*

Haotian Zheng, Kaiquan Wu, Jianou Huang, Yu Lei, Chao Li, Alexios Balatsoukas-Stimming, Zizheng Cao, and A. M. J. Koonen are with the Department of Electrical Engineering, Eindhoven University of Technology, 5612 AZ Eindhoven, The Netherlands (e-mail: c.li5@tue.nl; z.cao@tue.nl).

Bin Chen is with the School of Computer and Information, Hefei University of Technology, Hefei 230009, China.

Color versions of one or more figures in this letter are available at https://doi.org/10.1109/LPT.2020.3039177.

Digital Object Identifier 10.1109/LPT.2020.3039177

code of length N is constructed with a vector of relative reliabilities of bit indices $\mathbf{v} = \{v_0, \ldots, v_{N-1}\}$, where bit index v_i is less reliable than bit index v_j if $i < j$. The classical polar coding scheme divides all N source bits into two sets according to $\mathbf{v}$ and the number of unfrozen bits K. The set $\mathcal{A} = \{v_{N-K}, \ldots, v_{N-1}\}$ contains the indices of the K most reliable bits, while the set $\mathcal{A}_c = \{v_0, \ldots, v_{N-K-1}\}$ contains the indices of the remaining bits. The K unfrozen bit indices are assigned with r CRC bits and $K - r$ information bits. The $N - K$ frozen bit indices are set to fixed bits in advance, generally all zeros.

In order to achieve a reasonable error-correction performance for polar codes with finite length, CA-SCL decoding that follows the successive cancellation (SC) decoding schedule is used. If a bit with index $j \in \mathcal{A}$ is encountered in the decoding process, the decoding path will split by estimating the bit as either 0 or 1. Otherwise, the decoding path will extend by setting the bit to 0 directly. With the bit estimation, the path metric at each bit is calculated using an log-likelihood ratio (LLR)-based formulation [10]. At most L candidate paths with the best path metrics can survive at each bit estimation step. When all bits have been estimated, a CRC is executed on the final L candidate paths. The path with the minimum path metric amongst those that pass CRC is selected as the decoding output. If no path satisfies CRC, the one with the best path metric will be output.

B. Inter-Frame Polar Coding

1) Inter-Frame Correlated Encoding Scheme: In classical polar encoding scheme, the frozen bits in $\mathcal{A}_c$ are all zero-valued and the unfrozen bits in $\mathcal{A}$ are assigned $k - r$ information bits followed by r CRC bits. In inter-frame polar encoding scheme, the arrangement in the unfrozen part is the same as in classical scheme. However, the frozen bits are only partially zero-valued. The m most reliable frozen bits (MRFBs) in $\mathcal{A}_c^{\wedge} = \{v_{N-K-m}, \ldots, v_{N-K-1}\}$ of one frame are assigned with the value of the m most unreliable unfrozen bits (MUUBs) in $\mathcal{A}^{\vee} = \{v_{N-K}, \ldots, v_{N-K+m-1}\}$ of its preceding frame.

2) Inter-Frame Assisted Decoding Scheme: A detailed example is given for the decoding scheme. The decoding of the first frame is the same with the classical decoding. The CRC is verified to determine if the the decoding process succeeds. If it succeeds, decoding mode **M1** will be performed on the second frame. It also decodes K unfrozen bits and is only different from classical decoding in the values of MRFBs. They are assigned the values of MUUBs in the preceding frame instead of all zeros. Like this, if the decoding of the second frame succeeds, the decoding of the third frame will continue to use **M1**. Otherwise, the third frame will go to decoding mode **M2**, where $K + m$ bits will be decoded as unfrozen bits since the values of MRFBs cannot be obtained from the preceding frame. If the decoding of the third frame succeeds, its MRFBs will assist a re-decoding of the decoding failed second frame using decoding mode **M3**. As **M3** assigns the values of these MRFBs in the third frame to those of MUUBs in the second frame, the re-decoding only needs to decode $K - m$ unfrozen bits, which increases the successful decoding probability compared to **M1**. In this way, the frames help each other in decoding. The probability that the decoding of two adjacent frames both fail due to noise is low. Thus, the overall probability of decoding success will be improved.

C. Bit-Interleaved Polar-Coded Modulation

Bit-interleaved polar-coded modulation (BIPCM) is a common way to realize joint design of polar code and high-level modulation [11]. Conventional BIPCM uses an interleaver to improve the decoding performance. As shown in [6], the interleaver is unnecessary if the code construction takes the mapped bit-level difference into account. In our design, the MC method is applied in the code construction, which not only considers the mapped bit-level difference but also frequency selective fading on OFDM subcarriers. Thus, the orthogonal circulant matrix transform (OCT) used to overcome frequency selective fading in [6] is also unnecessary. MC method generates random information bits to calculate coded symbols repeatedly and transmit them over the ILC system. The received signals are fed into the soft demodulator to generate LLR of each bit by calculating:

$$L(X_i) = \ln\left(\frac{\sum_{X \in \mathbb{C}^{[i,0]}} P(Y|X)}{\sum_{X \in \mathbb{C}^{[i,1]}} P(Y|X)}\right), \tag{1}$$

where X_i denotes the i-th bit of the transmitted symbol X, $\mathbb{C}^{[i,b]}$ is the set of symbols whose i-th bit is equal to $b \in \{0, 1\}$. $P(Y|X)$ is the conditional probability of receiving Y as symbol X is transmitted. For simplicity, we approximate the channel as an additive white Gaussian noise (AWGN) channel, whose signal-to-noise ratio (SNR) equals the average SNRs of all OFDM subcarriers. After obtaining the channel LLRs in (1), they are input into the SC decoder to make bit-by-bit estimation assuming all previous bits are decoded correctly. The estimate is compared with the sent value for error detection of each bit. After transmitting enough coded symbols, the error probability of each polarized bit channel can be estimated with a ratio of the counted errors to the number of transmitted symbols. Consequently, the reliability of different bit indices can be sorted and the vector of relative reliabilities of bit indices $\mathbf{v}$ can be generated. This joint design of polar code and modulation using MC method is called MC-constructed polar coded modulation, where classical polar coding is employed. If the classical polar coding is replaced by inter-frame polar coding, the MC-constructed inter-frame polar coded modulation scheme is proposed as a result.

III. Experimental Setup and Results

The block diagram of the experimental setup for the 9.6 Gbit/s polar coded 16QAM OFDM-ILC system is shown in Fig. 1. Three kinds of coding schemes, namely, the classical MC-constructed polar coded modulation, the proposed MC-constructed inter-frame polar coded modulation and uncoded are investigated and compared in our experiments. Two code lengths of 512 and 1024 are considered in polar coding scheme. The used IFFT size is 512. Consider the Hermitian symmetry operation for an intensity modulation direct detection (IM/DD) system, only half subcarriers can be used. The first 8 subcarriers are set to zero to avoid the direct current (DC) influence and a maximum of 248 subcarriers can be used. Due to the frequency selective fading from optical devices in ILC system, high frequency components in OFDM symbols are suffered from low SNR. To get a reasonable performance and also accommodate with the code length,

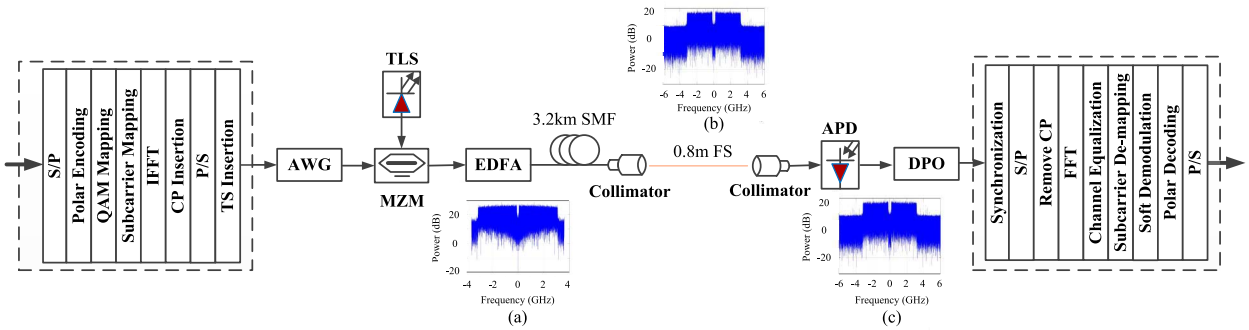

Fig. 1. Block diagram of inter-frame polar coded modulation OFDM-ILC system. (S/P = serial to parallel conversion, IFFT = inverse fast Fourier transform, TS = training sequence, AWG = arbitrary waveform generator, TLS = tunable laser source, MZM = Mach-Zehnder modulator, EDFA = Erbium Doped Fiber Amplifier, SMF = single-mode fiber, FS = free-space, APD = avalanche photodiode, DPO = digital phosphor oscilloscope, P/S = parallel to serial conversion.) (a), Electrical spectrum at BTB. (b), Electrical spectrum after SMF. (c), Electrical spectrum after SMF + FS.

we set the number of used subcarriers to the largest power of 2 less than 248, that is 128. In our system with 16QAM modulation and digital OFDM signal with 128 subcarriers loaded with data, one OFDM symbol carries 512 bits. Hence, the transmissions of 512 bits and 1024 bits codeword require 1 and 2 OFDM symbols, respectively. 10^4 codewords are generated offline for each code length. An arbitrary waveform generator (AWG) running at 12 GSa/s is used to produce the OFDM baseband signal, which then drives the Mach-Zehnder modulator (MZM). The effective bandwidth of the baseband OFDM signal is $128/512 \times 12 = 3$ GHz. With 16QAM modulation, we achieve a data rate of 12 Gb/s. The optical carrier with 10 dBm optical power is generated from a tunable laser source (TLS) at 1550 nm wavelength. The modulated optical signal is firstly amplified by an Erbium Doped Fiber Amplifier (EDFA), transmitted over 3.2 km single mode fiber (SMF), and then launched into the free-space (FS) via a fiber collimator with 10 dBm optical power. After 0.8 m FS link, the optical signal is coupled into a short section of SMF with more than 0 dBm optical power via another fiber collimator. It should be noted here that the free-space length is limited by the size of our lab table, but longer lengths using collimated narrow beam within a typical indoor room size would not result in significant performance variation [12]. At the receiver, the 16QAM OFDM signal is converted into electrical domain by an avalanche photodiode (APD) module, which is then sampled by a digital phosphor oscilloscope (DPO) at 25 GSa/s for further offline signal processing. The electrical spectrum of the OFDM signals at back-to-back (BTB), after transmission through the SMF, after transmission through the SMF and FS are demonstrated in Fig. 1 (a), (b), (c), respectively.

The construction of the polar codes depends highly on the channel. In this work, an indoor optical wireless channel combined with a section of SMF is adopted in the experiment. The target SNR is designed to be 14 dB, which corresponds to the received optical power (ROP) of -19 dBm in our experimental system. This SNR was targeted because the polar decoder requires a larger list size to achieve a reasonable performance for lower SNRs, while for the higher SNRs, more OFDM symbols are required to transmit to get an accurate bit error rate (BER) value. The code rates for the two code lengths are $R = 0.8$. Hence, the net data rate is 9.6 Gbit/s. It is shown in [10] that there exists a specific value of the parameter m with which the best error-correction performance can be achieved. The experiment sets $m = 15$ and 30 for $N = 512$ and 1024, respectively, which are firstly chosen through simulations and then by the experiments. For both the classical and proposed schemes, $L = 1$ and 2 are considered in CA-SCL decoding and CRC16-CCITT is adopted.

Fig. 2 shows the measured BER performance for different coding schemes as a function of the received optical power (ROP) at the code length of $N = 512$. The uncoded scheme retains a BER of about 1.2×10^{-2} around the designed operating point. As a comparison, the two schemes with polar coding show a significant performance improvement. It can be seen that the proposed scheme brings substantial performance gain in comparison with the classical scheme. At a ROP of -19 dBm, the proposed scheme with CA-SCL ($L = 2$) decoding achieves a BER of 2.3×10^{-5}, while that of its counterpart is 3.1×10^{-4}. As can be seen in the figure, this improvement decreases when the value of ROP deviates from -19 dBm. As the vector $\mathbf{v}$ changes with the deviation of ROP, the indices of bits in $\mathcal{A}$, $\mathcal{A}^{\vee}$, $\mathcal{A}_c$, $\mathcal{A}_c^{\wedge}$ selected for the designed operating point -19 dBm are no longer optimal at a different ROP. This also explains why some curves do not keep dropping with the increase of ROP. In addition, it can be observed that a larger list size leads to a larger performance gap between the classical and proposed schemes. As illustrated in Section II-B, the probability of successful decoding of **M2** will increase when using large list size, which leads to a higher probability of re-decoding for decoding failed frame. As a consequence, the overall average probability of decoding success will have a more pronounced improvement.

Fig. 3 displays the measured BER results at a code length of 1024 bits. Note that when measurements with no errors are observed, those are not included in the plot. Compared to Fig. 2, the performance gain brought by polar codes is higher at $N = 1024$ for both the classical and proposed schemes. Specifically, for the proposed scheme using CA-SCL ($L = 2$) decoding, measurements at a ROP of -19 dBm resulted in no errors over the approximately 10^7 bits, whereas errors were observed for the classical scheme. Note that the performance can be improved by increasing the value of L, while at the cost of higher complexity. Fig. 3 also shows the BER results at $N = 1024$ when codes optimized for each ROP are used. Significant improvement can be observed when comparing to those obtained using fixed code designed for ROP$= -19$ dBm. The performance of LDPC code with

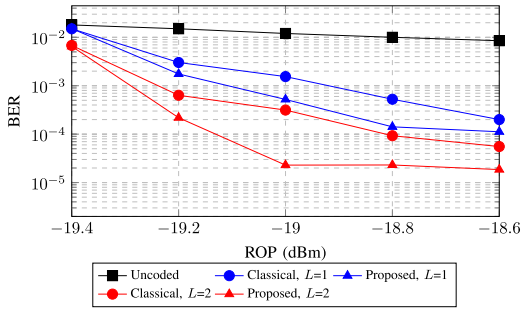

Fig. 2. Error-correction performance of the proposed scheme with $N = 512$, $R = 0.8$, $m = 15$ and designed ROP $= -19$ dBm.

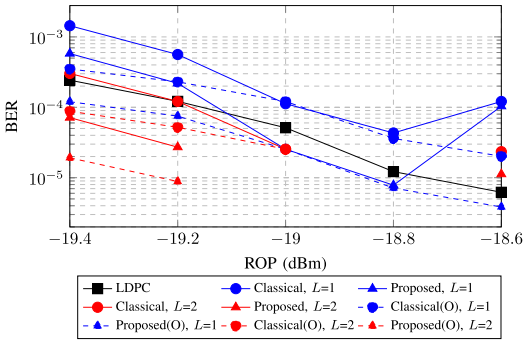

Fig. 3. Error-correction performance of the proposed scheme with designed ROP $= -19$ dBm, with codes optimized for each ROP (O), and LDPC code with $I = 2$, when $N = 1024$, $R = 0.8$, $m = 30$.

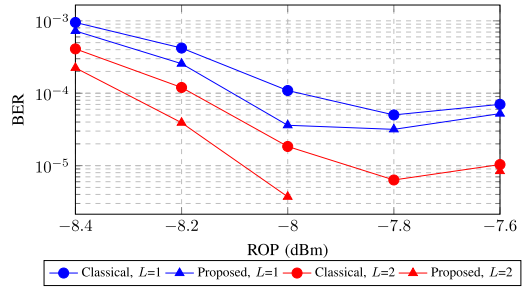

Fig. 4. Error-correction performance of the proposed scheme using 256QAM with $m = 30$, $N = 1024$, $R = 0.8$ and designed ROP $= -8$ dBm.

layered decoding algorithm (LDA) [8] and number of iterations $I = 2$ has been provided for comparison. We can find the performance of the proposed scheme outperforms that of LDPC when $I = L = 2$. Moreover, the performance advantage of the proposed scheme over the classical one can also be observed when 256QAM is adopted as shown in Fig. 4.

Table I reports the probability of re-decoding P_{re} and the normalized average and maximum computational complexity increment η_{aver} and $\eta_{\max}$ using CA-SCL ($L = 2$). $\eta_* = \left(\mathcal{C}^*_{prop} - \mathcal{C}^{aver}_{clas}\right)/\mathcal{C}^{aver}_{clas}$, where $\mathcal{C}^{aver}_{prop}$ and $\mathcal{C}^{max}_{prop}$ represents the average and maximum complexity of the proposed scheme, respectively, $\mathcal{C}^{aver}_{clas}$ denotes the average complexity of the classical scheme. The complexity is calculated in terms of the number of arithmetic operations required for the decoding of one frame by each scheme with $N = 512, 1024$ and CA-SCL ($L = 2$) decoding. As shown in Table I, while $\eta_{\max}$ is about 100%, η_{aver} is only up to 2.4% and 0.1% when $N = 512$ and 1024, respectively. It is worth mentioning that η_{aver} reduces as the code length or ROP increases. In terms of decoding latency, the maximum decoding latency of a frame is about twice as that of the classical scheme when re-decoding is executed. However, the increase in average latency is only up to 2.4% and 0.1% with respect to the classical counterpart when $N = 512$ and 1024, respectively.

TABLE I

PROBABILITY OF RE-DECODING AND NORMALIZED COMPUTATIONAL COMPLEXITY INCREMENT COMPARISON USING CA-SCL ($L = 2$)

	ROP (dBm)	−19.4	−19.2	−19	−18.8	−18.6
N=512	P_{re}	2.4%	0.3%	0.1%	0.06%	0.03%
	η_{aver}	2.4%	0.3%	0.1%	0.06%	0.03%
	$\eta_{\max}$	99.45%	99.45%	99.45%	99.45%	99.45%
N=1024	P_{re}	0.12%	0.06%	0.01%	0.005%	0.005%
	η_{aver}	0.12%	0.06%	0.01%	0.005%	0.005%
	$\eta_{\max}$	100%	100%	100%	100%	100%

IV. CONCLUSION

In this letter, an inter-frame polar coded modulation scheme is proposed and experimentally demonstrated in a 16QAM OFDM-ILC system with a net date rate of 9.6 Gbit/s. The experimental measurements show that the error-correction performance of the ILC system with the proposed inter-frame polar coded modulation scheme outperforms that of the classical counterpart significantly. Specifically, the proposed scheme employing a polar code of length 1024 and CA-SCL ($L = 2$) decoding resulted in no errors over 10^7 bits. In addition, it has an average decoding complexity which is only up to 2.4% higher than that of the classical scheme. Therefore, the proposed inter-frame polar coded modulation scheme is a promising candidate technology for indoor ILC systems.

REFERENCES

[1] T. Koonen, F. Gomez-Agis, F. Huijskens, K. A. Mekonnen, Z. Cao, and E. Tangdiongga, "High-capacity optical wireless communication using two-dimensional IR beam steering," *J. Lightw. Technol.*, vol. 36, no. 19, pp. 4486–4493, Oct. 1, 2018.

[2] J. M. Garrido-Balsells, A. Jurado-Navas, M. Castillo-Vázquez, and A. Puerta-Notario, "Improving RCPC codes in rate-adaptive optical wireless communications systems," *Wireless Pers. Commun.*, vol. 69, no. 2, pp. 879–889, Mar. 2013.

[3] L. Feng, R. Q. Hu, J. Wang, P. Xu, and Y. Qian, "Applying VLC in 5G networks: Architectures and key technologies," *IEEE Netw.*, vol. 30, no. 6, pp. 77–83, Nov. 2016.

[4] Z. Cao, J. Yu, W. Wang, L. Chen, and Z. Dong, "Direct-detection optical OFDM transmission system without frequency guard band," *IEEE Photon. Technol. Lett.*, vol. 22, no. 11, pp. 736–738, Jun. 1, 2010.

[5] E. Arikan, "Channel polarization: A method for constructing capacity-achieving codes for symmetric binary-input memoryless channels," *IEEE Trans. Inf. Theory*, vol. 55, no. 7, pp. 3051–3073, Jul. 2009.

[6] K. Wu, J. He, J. Ma, and Y. Wei, "A BIPCM scheme based on OCT precoding for a 256-QAM OFDM-VLC system," *IEEE Photon. Technol. Lett.*, vol. 30, no. 21, pp. 1866–1869, Nov. 1, 2018.

[7] J. Ma *et al.*, "Performance enhanced 256-QAM BIPCM-DMT system enabled by CAZAC precoding," *J. Lightw. Technol.*, vol. 38, no. 3, pp. 557–563, Feb. 1, 2020.

[8] T. Koike-Akino *et al.*, "Bit-interleaved polar-coded modulation for low-latency short-block transmission," in *Proc. Opt. Fiber Commun. Conf.*, 2017, p. W1J-6.

[9] H. Zheng, S. A. Hashemi, B. Chen, Z. Cao, and A. M. J. Koonen, "Inter-frame polar coding with dynamic frozen bits," *IEEE Commun. Lett.*, vol. 23, no. 9, pp. 1462–1465, Sep. 2019.

[10] A. Balatsoukas-Stimming, M. Bastani Parizi, and A. Burg, "LLR-based successive cancellation list decoding of polar codes," *IEEE Trans. Signal Process.*, vol. 63, no. 19, pp. 5165–5179, Oct. 2015.

[11] M. Seidl, A. Schenk, C. Stierstorfer, and J. B. Huber, "Polar-coded modulation," *IEEE Trans. Commun.*, vol. 61, no. 10, pp. 4108–4119, Oct. 2013.

[12] K. A. Mekonnen, J. H. C. van Zantvoort, N. Calabretta, N. Tessema, E. Tangdiongga, and T. Koonen, "High-capacity dynamic indoor network employing optical-wireless and 60-GHz radio techniques," *J. Lightw. Technol.*, vol. 36, no. 10, pp. 1851–1861, May 15, 2018.